infrastructures

MDPI

Article

Pultruded GFRP Girders for the Replacement of Deteriorated Concrete Bridges

Giuseppe Campione and Michele Fabio Granata *

Dipartimento di Ingegneria, Università di Palermo, 90128 Palermo, Italy; giuseppe.campione@unipa.it
* Correspondence: michelefabio.granata@unipa.it

Abstract

This paper investigates lightweight structural systems based on pultruded GFRP girders for the replacement of deteriorated concrete bridge decks on existing piers and abutments. The study is motivated by the need to rehabilitate short- and medium-span bridges affected by aging deterioration such as reinforcement corrosion. The approach preserves existing piers and foundations and, when required, enables rapid deployment for temporary or emergency applications. The proposed GFRP deck–girder solutions significantly reduce structural mass compared to conventional concrete systems. This reduction leads to lower seismic demand and smaller horizontal forces transmitted to the substructures. The research assesses the structural performance and feasibility of these systems, with particular attention to strength and serviceability behavior. The objective is to identify solutions that can be replicated across different bridge configurations, while also outlining efficient strategies for onsite assembly. After a reasoned review of the solutions available in the literature and of the limitations related to deformability, strength, and instability for a preliminary analytical design approach, three-dimensional numerical simulations of GFRP bridge deck systems are performed to evaluate global behavior and load-transfer mechanisms. The latest design codes and guidelines for GFRP bridges are reviewed and applied. Based on the results, recommendations are provided regarding cross-sectional proportions and member slenderness. The numerical results are compared with the analytical design approach, showing that, under characteristic load combinations, maximum deflections can be limited to approximately L/300–L/400 when the beam depth-to-span ratio range is between 1/10 and 1/6. Within these relationships, spans between 10 m and 25 m are found to be efficient. Additional guidance is proposed for modular construction strategies based on standardized pultruded elements and factory-controlled bonded connections.

Keywords: GFRP bridge; buckling; lightweight deck; long-term effects; shear deformation

Academic Editors: Miao Su, Zhiping Zeng, Min Wu and Fuming Wang

Received: 13 March 2026
Revised: 30 March 2026
Accepted: 2 April 2026
Published: 3 April 2026

1. Introduction

The use of fiber-reinforced polymer (FRP) composites in pedestrian and road bridges has gained increasing attention over the past decades, either for complete structural systems or for specific components such as trusses, girders, and deck panels. Among them, glass fiber-reinforced polymer (GFRP) pultruded profiles demonstrated significant potential due to their low self-weight, ease of handling, and suitability for rapid construction [1,2], making them attractive for reducing the dead load of bridge superstructures and the demand on foundations and abutments [3]. Compared to conventional steel or prestressed concrete bridges, the reduction in dead loads achieved using GFRP members represents a clear advantage, especially in rehabilitation projects or where soil conditions or construction constraints limit the applicability of traditional materials [4].

Pultruded GFRP structural elements are manufactured through automated industrial processes combining continuous glass fibers and polymeric matrices, resulting in one-dimensional members with cross-sectional geometries closely resembling those of traditional steel carpentry. These profiles are characterized by a much lower specific weight than steel and by high resistance to corrosion and aggressive environmental agents, which can significantly enhance durability and reduce maintenance requirements [5]. Although the initial cost of GFRP bridge components is generally higher than that of steel, life-cycle cost analyses have shown that GFRP solutions can be economically competitive when durability and reduced maintenance are considered, particularly for bridge decks, whose expected service life may be several times longer than that of reinforced concrete members [1,2].

Despite these advantages, the structural design of GFRP bridge systems is typically governed by Serviceability Limit States rather than ultimate strength. This is primarily due to the relatively low elastic modulus of GFRP composites compared to steel, combined with pronounced time-dependent effects such as creep and stress relaxation [1]. Consequently, deflection limits often control the sizing of GFRP decks and girders, particularly under sustained or point loads. Additional drawbacks include sensitivity to viscous effects, limited fire resistance, brittle failure behavior, and second-order effects. Moreover, the low mass and stiffness of GFRP structures may lead to unfavorable dynamic performance, making them susceptible to vibrations induced by pedestrian or vehicular traffic [1,6].

To date, most realized GFRP bridge applications involve pedestrian bridges, typically designed for live loads between 3 and 5 kN/m^2, with spans ranging from 10 to 20 m and structural systems based on full-web or lattice beams with depths of approximately $1 \div 2$ m [2,3,7]. In contrast, the application of GFRP systems in road bridges remains limited. Road bridges are subject to significantly higher live loads, commonly between 15 and 30 kN/m^2, as well as strict serviceability requirements, with maximum allowable deflections typically ranging from L/300 to L/600. These constraints often lead to oversized structural members, which reduces the economic competitiveness of GFRP solutions and confines their use to specific scenarios where steel or concrete structures are less suitable, such as highly corrosive environments or emergency replacement situations [5,8].

Although the use of pultruded GFRP in bridge engineering is still limited, several design standards and pre-code documents are currently available and provide guidance for verification in both Ultimate and Serviceability Limit States. Notable references include Eurocomp (1996) [9], Highway Structures and Bridge Design (2005) [10], CNR-DT 205 (2008) [11], AASHTO LRFD specifications (2010) [12], AASHTO guidelines on tubular sections (2013) [13], ASCE/SEI 74 (2023) [14], and recent CEN provisions (2022) [15] or Chinese recommendation T/CECS 692-2020 [16]. Nevertheless, uncertainties related to long-term behavior, structural redundancy, and connection performance continue to represent major barriers to widespread adoption.

Among the structural typologies suitable for GFRP bridges, truss systems are particularly attractive due to their efficient use of materials and favorable strength-to-weight ratio. However, experimental and numerical investigations have shown that GFRP truss members are highly sensitive to compressive stresses, exhibiting susceptibility to local and global buckling, as well as significant creep effects under sustained loading (Yang et al. [17]; Zhu et al. [18]; Barbero & Tomblin [19]; Puente et al. [20]; Pecce & Cosenza [21]). Furthermore, connections have been consistently identified as the most critical components, governing overall structural performance. Bolted connections require drilling operations that introduce stress concentrations, local damage, and hole ovalization, leading to a substantial reduction in load-bearing capacity, often more pronounced than in comparable steel joints (Higgoda et al. [22]; Chen et al. [23]; Bai & Yang [7]). Adhesively bonded joints, while avoiding stress concentrations, may suffer from delamination, peeling, and punching failures, which can severely compromise the structural integrity and reliability of GFRP members [2,4].

The main aim of this study is to develop feasible GFRP deck solutions for road bridges that can replace existing concrete superstructures while utilizing the original substructures (piers, abutments and foundations). The inherent lightness of GFRP members, combined with their ease of handling and assembly, makes them particularly suitable for the rapid replacement of damaged bridges, minimizing disruption to traffic and infrastructure. In fact, aging bridges can present advanced degradation and damage to deck superstructures due to reinforcement corrosion, especially when they are placed near the sea, both for ordinary RC structures and prestressed girders [24,25]; hence, in some cases, it is not possible to rehabilitate the existing deck, and it is more convenient to replace it.

In particular, the primary advantage of replacing a heavy reinforced concrete deck with a GFRP deck, which is extremely lightweight, lies in the possibility of retaining the existing substructures (piers, abutments, and foundations) without the need for strengthening or upgrading. This aspect is especially critical in seismic regions, where deficiencies in the substructures would otherwise lead to complete bridge replacement or require complex seismic retrofitting solutions. In contrast, the reduction in structural mass and in the reaction forces transmitted to supports significantly decreases the strength demand on the existing substructures, making their continued use feasible without rehabilitation.

This approach enables a much faster deck replacement process, and the higher initial cost associated with GFRP deck systems is offset by the ease of prefabrication, assembly, and installation, the reduced need for heavy launching equipment due to the lower self-weight, and the elimination of works involving the substructures, which remain in place. As a result, an overall economic benefit can be achieved, balancing the higher material cost of pultruded GFRP elements with the reduced costs associated with demolition, reconstruction, launching operations, and strengthening of the existing supporting and foundation structures.

The study presented herein is structured in a two-stage approach. In the first stage, the essential aspects of GFRP deck design are addressed using simplified and expedient methods for preliminary sizing. This involves evaluating the structural typology of the deck, ensuring adequate strength, stiffness, and stability, and selecting appropriate connection strategies that facilitate rapid assembly while maintaining structural integrity. Special attention is given to the design of joints between primary load-bearing beams and the deck panels, as these connections are critical for both performance and constructability [21,26].

In the second stage, the proposed deck solution is examined through a detailed three-dimensional finite element (3D FE) analysis. This simulation accounts for the full three-dimensional behavior of the deck, including global deformability, load redistribution, and stress patterns under both permanent and variable traffic loads [16,17,27]. The interaction between structural members is explicitly modeled, allowing an accurate assessment of the structural response and the effectiveness of the proposed connection solutions [4,28].

Through this integrated methodology, the study establishes a comprehensive framework for the design of structurally efficient GFRP bridge decks suitable for the rapid replacement of damaged concrete bridges, providing guidance on both preliminary sizing and detailed numerical evaluation, while emphasizing connection detailing and assembly strategies for real-world applications and, as its principal novel contribution, extending such practical design guidance to trussed GFRP bridge decks with typical spans for RC road bridges, where current engineering applications remain largely confined to pedestrian bridges.

2. Preliminary Design of the Main Deck Superstructure

This section focuses on the specific design considerations for sizing GFRP bridge deck elements. Figure 1 illustrates the concept, showing a representative GFRP truss bridge designed to replace a deteriorated reinforced concrete superstructure while reusing the existing piers and foundations. The substantially reduced self-weight of the GFRP deck not only facilitates construction but also contributes to meeting the seismic retrofit requirements of the substructure [29]. The analysis presented here is based on relevant design codes and the specialized literature and proposes selected refinements to the analytical assessment procedures. These refinements have been validated against experimental and numerical data reported in the literature and specifically tailored to the structural problem addressed in this study.

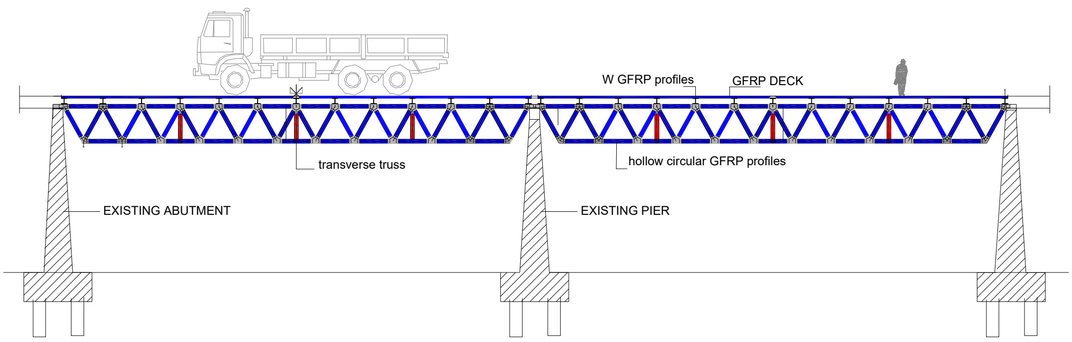

Figure 1. Example of replacement of an existing R.C. bridge through a trussed GFRP deck.

2.1. *Review of Literature Research on GFRP Pultruded Trusses for Bridge Decks*

Several experimental studies, over the past decades, have investigated the structural behavior of GFRP truss systems [17,18,22,23]. Table 1 summarizes the key characteristics of truss elements with hollow circular and square cross-sections used in these investigations.

Yang et al. [17] developed space trusses with a span of 8 m, width of 1.13 m, and depth of 1.60 m, composed of pultruded circular hollow section (CHS) members with a diameter of 92 mm and wall thickness of 8 mm. Members were connected to aluminum nodes using steel joint plates and two M16 bolts, while GFRP tubes were bonded to steel sleeves welded to the plates using a two-component epoxy adhesive (Araldite 420 A/B). The GFRP exhibited a compressive strength of 300 MPa and an axial modulus of 39.3 GPa, while the adhesive had a tensile strength of 28.6 MPa, tensile modulus of 1.9 GPa, and shear strength of 25 MPa. Three-point bending tests revealed a linear load–displacement response up to buckling and longitudinal splitting of the upper compressive members, with a peak load of 164 kN and a corresponding deflection of 45 mm.

Zhu et al. [18] studied space trusses with a width of 1.60 m and depth of 1.23 m, consisting of pultruded CHS members with a diameter of 60 mm and wall thickness of 6 mm, connected to aluminum nodes. Three-point bending tests exhibited linear elastic behavior until the buckling and splitting of the compressive members, with a peak load and deflection similar to those reported by Yang et al. [17].

Higgoda et al. [22] investigated 4.5 m long space frames in which diagonal braces were adhesively bonded directly to the chords. The GFRP material had a compressive strength of 485 MPa, with the axial and transverse moduli E_1 = 33 GPa and E_2 = 11.9 GPa, and the shear modulus G = 4.2 GPa. Upper and lower chords had a diameter of 114 mm and wall thickness of 6.4 mm, while diagonal and vertical braces measured 50 mm in diameter and

3.2 mm in thickness. Four concentrated loads were applied during testing, and almost linear behavior was observed up to failure, which occurred at a total load of 34.9 kN and a deflection of 12 mm, primarily due to the detachment of a diagonal brace near the support.

Table 1. Truss structures tested in the literature.

<table>
<tr><th>Author</th><th>Prototype of Truss</th></tr>
<tr><td>Yang et al. [17]
(2015)</td><td>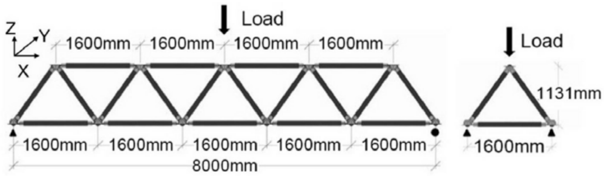</td></tr>
<tr><td>Zhu et al. [18]
(2020)</td><td>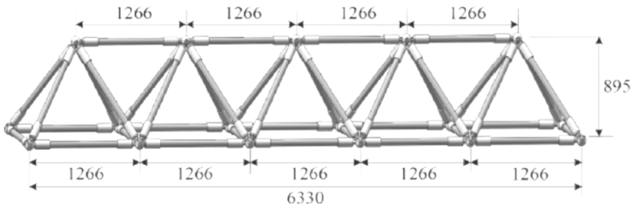</td></tr>
<tr><td>Higgoda et al. [22]
(2022)</td><td>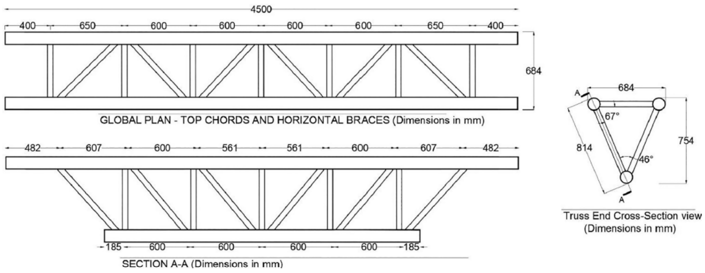</td></tr>
<tr><td>Chen et al. [23]
(2022)</td><td>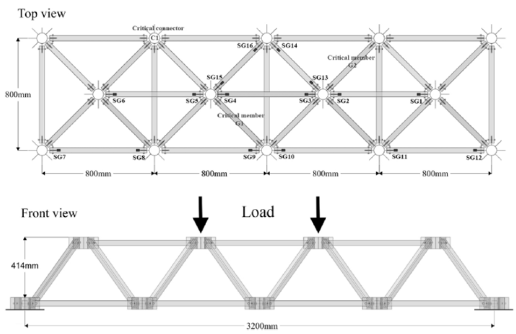</td></tr>
</table>

Chen et al. [23] examined similar 4.5 m long space frames, where diagonal braces were connected to steel plates with two M16 bolts. Members had square cross-sections (40×5 mm) with a compressive strength of 337.5 MPa, axial modulus E_1 = 37.6 GPa, and shear modulus G = 2.5 GPa. Failure modes included bolt shear and fiber lamination. Three-point bending tests showed a maximum load of 29.2 kN and a corresponding deflection of 15.9 mm.

These experimental tests show the importance of bolt connections and arrangement of structural members in the truss girder [29–31] for shear–flexure strength.

2.2. Design for Strength and Local Buckling

For preliminary design, the main references are ASCE/SEI 74 [14] and CEN Provisions [15], particularly for the strength check of structural elements in GFRP bridge systems. Regarding the tensile and compressive strength of GFRP materials, both ASCE and the CEN Provisions prescribe that these properties be determined through appropriate experimental testing, providing material-specific strength values to be adopted in design and check procedures. In addition, several studies available in the literature propose correlations between the compressive strength of GFRP and its shear modulus G. Cardoso et al. [30] provide an example, where this relationship is expressed in the following form:

$$\sigma_m = 0.107 \cdot G \tag{1}$$

Since the shear modulus G is correlated with the longitudinal elastic modulus E_1, and considering that the longitudinal behavior of the bridge represents the governing aspect of the structural response, especially from the deflection point of view, a correlation between the compressive stress and the longitudinal elastic modulus is herein proposed, expressed through the following relationship:

$$\sigma_m = \frac{E_1}{135} \quad [\text{MPa}] \tag{2}$$

where E_1 is the longitudinal elastic modulus in compression.

By compiling the experimental results reported by Teixeira et al. [27], Higgoda et al. [22], Hizam et al. [30,31], Bacinskas et al. [32], Yang et al. [17], and Kim et al. [26], the dataset illustrated in Figure 2 is obtained. The relationship between the compressive strength of GFRP and the corresponding elastic modulus in compression is highlighted, as derived from a broad range of experimental investigations available in the literature. The same figure also reports the formulation proposed by Cardoso et al. [33], evaluated by assuming a shear modulus equal to $G = 1/9 \cdot E_1$. A comparison between the experimental data and the analytical expressions indicates that the correlation proposed in the present study through Equation (2) provides a closer agreement with the experimental results than Equation (1), particularly within the range of elastic moduli relevant to the structural elements under investigation. The regression used for fitting experimental data has a mean value of 0.905, standard deviation of 0.176 and covariance of 0.194.

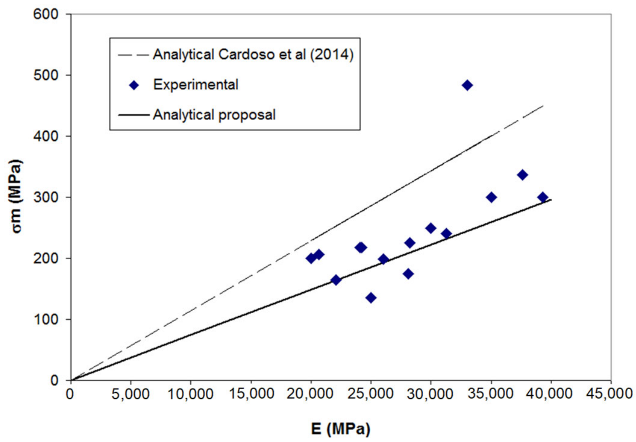

Figure 2. Variation in GFRP compressive strength with elastic modulus in compression.

In accordance with ASCE/SEI 74 [14] and the CEN Provisions [15], truss elements subjected to tensile forces—such as lower chords under vertical load effects, as well as selected diagonal and vertical members acting as ties—are verified on the basis of the effective cross-sectional area, defined as the gross area reduced by the area of bolt holes, where applicable, and by adopting the tensile design strength of the GFRP material.

For the upper chords and selected diagonal and vertical members of the truss, which must be designed to carry compressive forces, the critical stress needs to be evaluated to assess the onset of instability. This evaluation can be performed experimentally through stub column tests, numerically via finite element analyses, or analytically using available expressions from the literature.

The analytical formulations typically used for this purpose are derived from the classical solution proposed by Timoshenko and Gere [34] for the elastic buckling of a compressed cylindrical member made of homogeneous and isotropic material. These formulations have been adapted to account for the anisotropic behavior of GFRP by introducing distinct longitudinal and transverse elastic moduli (E_1, E_2), as well as the corresponding Poisson ratios (ν_{12} and ν_{21}).

The expression for the critical compressive stress of circular hollow truss members has been proposed through different expressions, ranging from simplified approximations to more detailed formulations. In accordance with the recommendations of Eurocomp [9], the critical compressive stress is

$$\sigma_{cr} = 0.250 \cdot E_1 \cdot 2 \cdot t/D \tag{3}$$

where t is the thickness and D is the diameter of the hollow section. Equation (3) accounts only for the elastic modulus in the longitudinal direction.

According to ASCE/SEI 74 [14], the critical stress is instead related to longitudinal and transverse moduli, and it can be calculated as

$$\sigma_{cr} = \frac{2 \cdot t}{D} \cdot \min\left(\sqrt{\frac{E_1 \cdot E_2}{3}}; \sqrt{\frac{2}{3} \cdot G \cdot \sqrt{E_1 \cdot E_2}}\right) \tag{4}$$

while AASHTO [13] suggests calculating critical stress with the expression

$$\sigma_{cr} = 0.75 \cdot \frac{E_1}{\left(1 - \nu_{12}^2 \cdot E_2/E_1\right)^{0.5}} \cdot \frac{t}{D} \cdot 1.414 \cdot \left[\left(1 + \nu_{12} \cdot \left(\frac{E_2}{E_1}\right)^{0.5}\right)\left(\frac{E_2}{E_1}\right)^{0.5}\left(\frac{G}{E_1}\right)\right]^{0.5} \tag{5}$$

Finally, Campione [4] suggested the following expression:

$$\sigma_{cr} = \left[2 \cdot \frac{t}{D} \cdot \sqrt{\frac{E_1 \cdot E_2}{3 \cdot \left(1 - \nu_{12}^2\right)}}\right] \cdot \sqrt{0.625 \cdot \left(\frac{E_2}{E_1}\right)^{0.85}} \tag{6}$$

By expressing the critical stress in terms of the longitudinal elastic modulus through Equation (2) and equating each of the expressions (3)–(6) above to Equation (2), it is possible to obtain several limiting values of the D/t ratio between the diameter and the thickness of the hollow profile, corresponding to the attainment of the critical stress, that is, to avoid local buckling before crushing in compression. Table 2 supplies the D/t ratios for the different expressions used, by varying the elastic moduli ratios: E_2/E_1 = 1, 1/3 and 2/3; G = 1/9 E_1; ν_{12} = 0.25.

Table 2. Maximum geometrical slenderness of a circular hollow cross-section.

Reference	**D/t**		
	$E_2 = E_1$	**E_2 = 1/3 E_1**	**E_2 =2/3 E_1**
Eurocomp (1986) [9]—Equation (3)	50	50	50
ASCE/SEI 74 (2023) [14]—Equation (4)	54	41	49
AASHTO (2013)[13]—Equation (5)	50	39	46
Campione (2025) [4]—Equation (6)	93	33	64

Figure 3 presents a comparison between Equations (4) and (6), which describe the variation in the critical stress as a function of the D/t ratio. The analysis is performed for a material characterized by E_1= 27 GPa, E_2/E_1 = 1/3 and G = 1/9 E_1. The same figure also reports the experimental data obtained by Yazhini & Ramesh [35], Yang et al. [17], and Yousif et al. [36] for hollow circular cross-sections. The comparison indicates that the ASCE/SEI 74 [14] formulation tends to overestimate the critical stress in certain cases, whereas the one by Campione [4] provides closer agreement with the available experimental data.

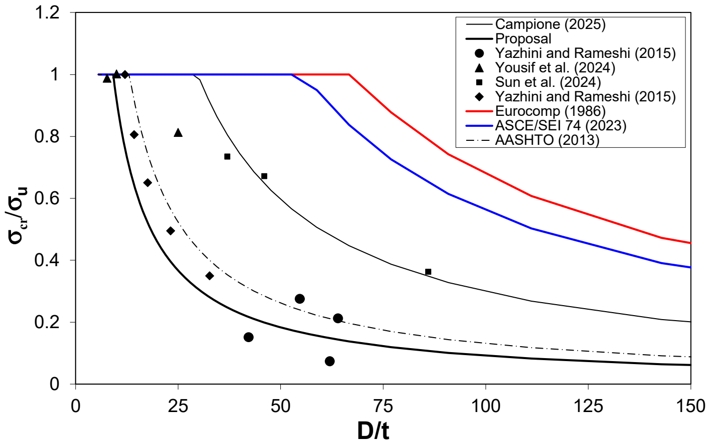

Figure 3. Variation in critical stress with D/t ratio for circular hollow cross-section.

Although this may appear at first glance to be a reduction in the safety factor compared with more conservative code-based curves, it should be noted that the improved fitting to the experimental data remains very close to the AASHTO curve, while providing a better representation of all data points across the full range of critical-to-ultimate stress ratios. In contrast, some curves available in the literature do not fully capture the experimental trends, either providing satisfactory fitting only for a limited subset of data within a specific thickness range or leading to overly conservative *D/t* requirements, which could supply overestimated profile dimensions associated with insufficient thickness.

2.3. Design for Global Instability

Once the correlation between the cross-sectional geometry, the critical stress, and the material mechanical properties has been established, the next step is to assess the slenderness of the structural member and in particular the compressed bars within the truss. Specifically, it is necessary to evaluate the global instability of the member once the local buckling of the section has been verified. To this aim, reference is made to the Euler critical load, based on the mechanical slenderness λ_c or the geometrical slenderness λ, defined as

$$\lambda_c = \sqrt{\frac{\min(\sigma_{cr}, \sigma_m) \cdot A}{P_e}}, \lambda = \frac{l_0}{(J/A)^{0.5}} \tag{7}$$

where A, J are the cross-sectional area and minimum inertia, P_e is the critical Euler load, and l_0 is the effective length. For the calculation of the critical load of slender elements, ASCE/SEI 74 [14] adopts Euler's expression in the following form:

$$P_e = \frac{\pi^2 \cdot E \cdot J}{l_0^2} \tag{8}$$

Through Equation (8), by equating the critical stress to the material compressive strength, the limiting slenderness of the compressed member is obtained, which is found to be 36.48. It is well established in the literature that, for members with high slenderness, the Euler-predicted critical load must be corrected to account for the shear contribution, as follows:

$$P_{Eg} = P_e \cdot \frac{1}{1 + k \cdot P_e/(G \cdot A)} \tag{9}$$

The values of k adopted in Equation (9) are those suggested by Timoshenko and Gere [34] for isotropic material and for a thin-walled circular section of a solid tube. They are equal to 0.5 and 0.75, respectively, and 5/6 for W shapes.

In pultruded members, due to the presence of initial imperfections, an interaction occurs between local and global buckling. To account for this phenomenon, ASCE/SEI 74 [14] proposes evaluating the critical load as follows:

$$P_{cr} = \sigma_{cr} \cdot A \cdot \frac{1 + 0.12 \cdot \left(\lambda^2 - 0.25\right) + \lambda^2 - \sqrt{1 + 0.12 \cdot \left[\left(\lambda^2 - 0.25\right) + \lambda^2\right]^2 - 4 \cdot \lambda^2}}{2 \cdot \lambda^2} \tag{10}$$

Hence, the ultimate load in compression P_u of the truss member, according to ASCE/SEI 74 [14], is the minimum among $P_1 = \sigma_{cr}\, A$ (where σ_{cr} is evaluated through Equation (4)), P_e from Equation (7) and P_{cr} from Equation (10). Alternatively, CEN Provisions [15] also calculate the ultimate load with the following expression:

$$N_{C,RD} = \frac{1}{0.65 \cdot \lambda_c^2}\left(\frac{1+\lambda_c^2}{2} - \sqrt{\left(\frac{1+\lambda_c^2}{2}\right)^2 - 0.65 \cdot \lambda_c^2}\right) \cdot N_{loc,RD} \tag{11}$$

where $N_{loc,RD}$ is the design value of the compressive force corresponding to the onset of local instability of the profile, which can be determined either through experimental tests on stub elements or via numerical–analytical modeling.

Figure 4 illustrates the variation in the ultimate stress as a function of the geometrical slenderness, according to the different models considered (Equations (8)–(11)). Theoretical predictions were obtained, assuming E_1 = 27 GPa, E_2 = 1/3 E_1, G = 1/9 E_1 and ν = 0.25. The figure also includes the experimental data reported by Zhang & Li [27] and Zhang et al. [28]. The comparison indicates that most of the considered models are able to predict experimental results with satisfactory accuracy, capturing the overall trend of the ultimate stress as a function of slenderness. Minor deviations between the theoretical and experimental values can be attributed to inherent material variability, geometric imperfections, and potential boundary condition effects. Overall, the agreement confirms the reliability of the theoretical formulations for estimating the ultimate stress of slender pultruded members under compression.

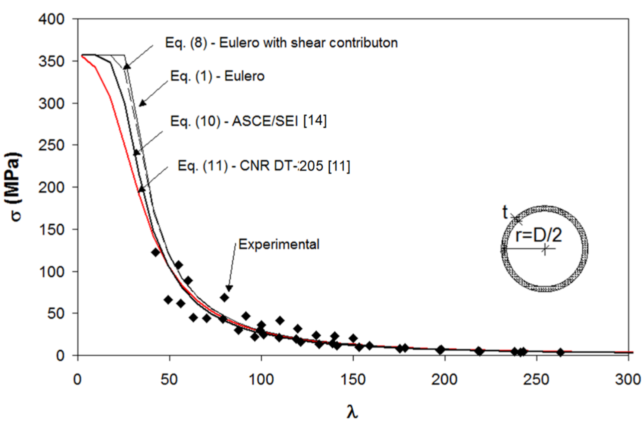

Figure 4. Global critical buckling stress versus mechanical slenderness.

3. Example of Design of a Pultruded GFRP Bridge

3.1. Sizing Aspects and Analytical Approach to Design

In this section, an example of a road bridge is presented (see Figure 5). The bridge consists of a spatial GFRP truss of height h, simply supported at the ends, arranged longitudinally with a span L and width B. Longitudinal main trusses are connected by transverse trusses located at $L/3$, $L/2$ and $2/3L$. At each joint, upper W-shaped profiles are provided, and the structure is completed with a GFRP deck placed on top of the trusses.

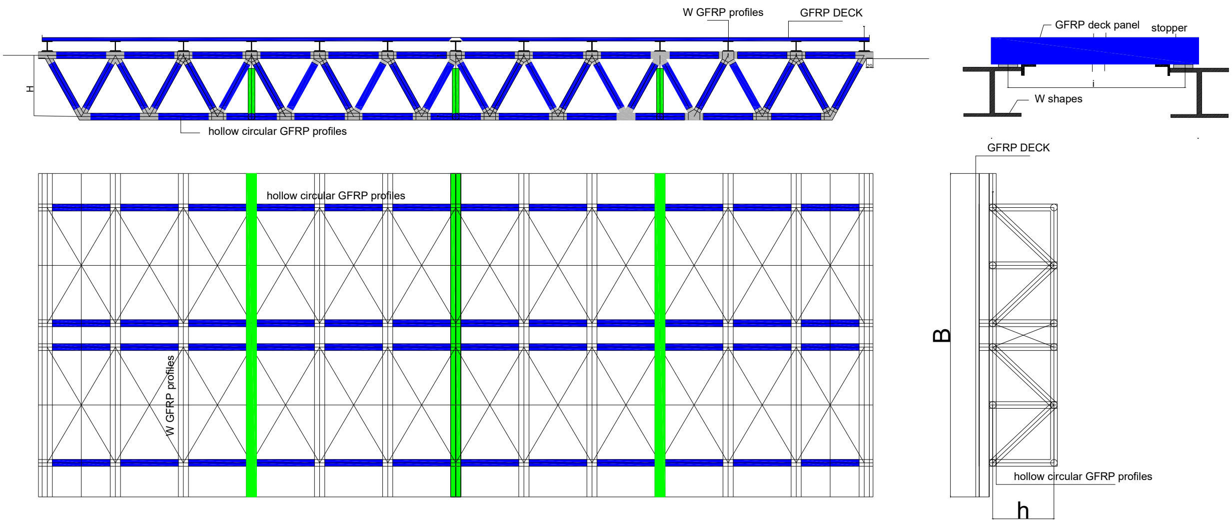

Figure 5. Proposal of pultruded GFRP bridge.

The bridge truss configuration shown in Figure 5 was selected to enable all horizontal members to have equal lengths for a given height of the main longitudinal truss. This design strategy simplifies fabrication and assembly and facilitates quality control of the structural elements, which can be partially conducted in the factory using nondestructive techniques such as ultrasonic testing. Furthermore, the transverse trusses are connected to the primary longitudinal truss using the same joint system adopted for the longitudinal plane connections, as illustrated in Figure 6. This approach ensures uniformity in joint design, enhances structural consistency, and simplifies the overall construction process.

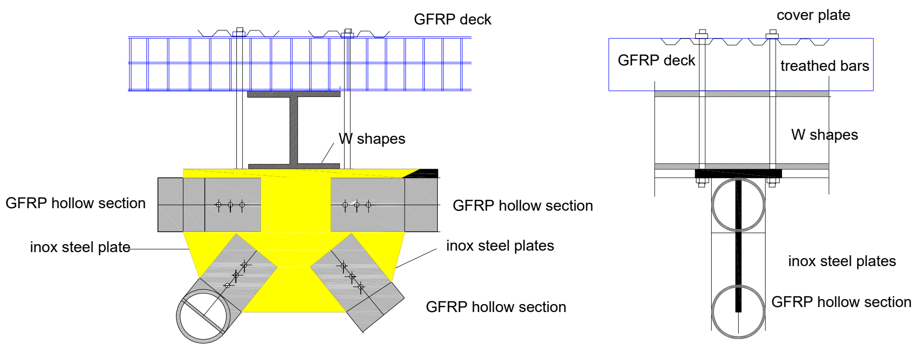

Figure 6. Proposed deck-to-girder connection and truss elements in the joint connection.

The choice of a circular cross-section instead of a W-shaped profile is motivated by the need to bond GFRP elements to stainless steel tubes without using bolts.

Conversely, the use of a closed cross-section may lead to the accumulation of impurities inside the profile, potentially causing further degradation. However, this can be accounted for in the service life of the elements and is considered acceptable if the bridge is designed for a service life of about 10 years. The design of the diagonals and transverse trusses follows the same procedure applied to the primary truss elements.

The deck adopted is that shown in Figure 7, as studied by Kim et al. [26]. The GFRP deck has a cross-sectional depth of 750 mm, a thickness of 200 mm, and a span of 2000 mm. The parameters t_{w0}, t_{wi} and t_f correspond to the thicknesses of the outer web, inner web, and flange, respectively. The top flange is assumed to have the same thickness as the bottom flange, allowing the panel to be inverted if one side deteriorates. The outer web is slightly thicker than the inner web to account for its greater tendency to wear during service.

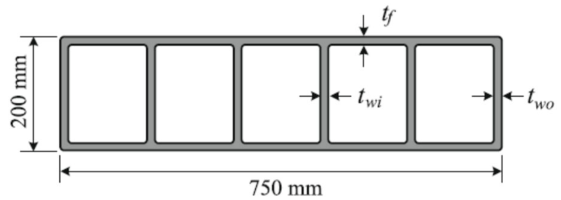

Figure 7. GFRP deck adopted for the proposed truss bridge.

The connections between the FRP deck and the W-shaped girders in the adopted system utilize the shear-pocket confinement method (see Figure 6), as proposed by Kim et al. [26]. In this method, a series of shear studs are inserted into pockets prepared within the cellular FRP deck, and the pockets are subsequently grouted to provide confinement. W-shaped GFRP beams are connected to the steel plates of the truss joints using externally bolted treated bars, as illustrated in Figure 6.

Each truss member, which is theoretically subjected only to axial tension or compression, is connected at the joints. The joints are assumed to behave as frictionless hinges or pins, allowing slight rotation at the member ends and ensuring a stable structural configuration. The connections between truss elements are realized as shown in Figure 8, with steel plates joined by bolts (Bai & Yang, [7]; Hizam et al. [30]; Hao et al. [37]; Qiu et al. [38]). The GFRP elements are bonded to stainless steel tubes inserted within the GFRP profiles.

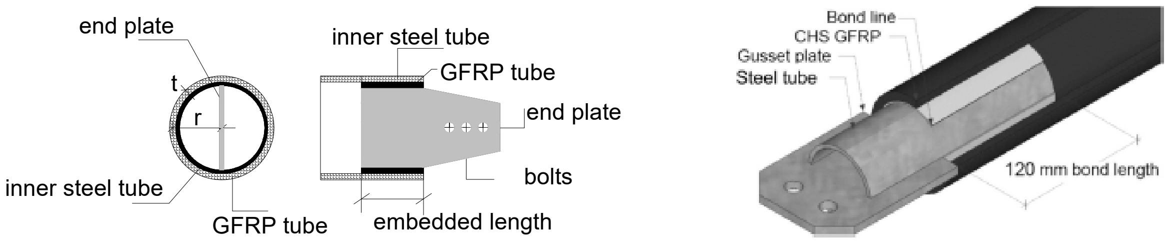

Figure 8. Proposal for joint connection for hollow circular cross-sections.

The required bonded length can be determined following the Italian guidelines of CNR-DT 205 [11] or experimental studies (e.g., Yang et al. [16]; Zhu et al. [17]), for which bonded lengths have been adopted ranging between 100 and 120 mm. The steel tubes are welded to the steel plates, which are then connected to the joints using high-strength bolts, as illustrated in Figure 8.

According to Eurocode 1 [39], the uniformly distributed design load of the road bridge is 9 kN/m^2 for the most loaded lane, in addition to the tandem point loads (300 kN). For the preliminary design, simply supported beams are considered, with a moment of inertia J and section modulus W equivalent to those of a single longitudinal truss constituting the bridge, with the cross-sectional type reported in Table 3. For the simply supported beam, the strength and deformability checks are based on the use of the following expressions giving the required strength modulus and inertia for a given design strength f_{yd} and deflection limit δ_0. The strength modulus is

$$W_e = \left(\frac{1}{2} \cdot q_{ULS} \cdot L + P_{ULS}\right) \cdot \frac{L}{4 \cdot f_{yd}} \tag{12}$$

where q_{ULS} and P_{ULS} are respectively distributed and point loads in Ultimate Limit State. Deflection is

$$\delta = \frac{L^3}{8 \cdot E_1 \cdot J}(5 \cdot q_{SLE} \cdot L + P_{SLE}) + \frac{L}{4 \cdot \chi \cdot G \cdot A}\left(\frac{1}{2} \cdot q_{SLE} \cdot L + P_{SLE}\right) \leq \delta_0 \tag{13}$$

where q_{SLE} and P_{SLE} are the distributed and point loads in Serviceability Limit State.

Table 3. Properties of truss cross-section.

Truss Solution		**(a)**	**(b)**	**(c)**
Properties		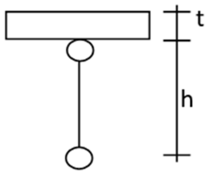	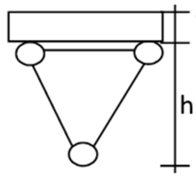	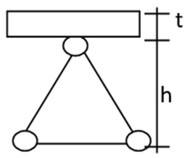
Without deck	A_t	$2\,A$	$3\,A$	$3\,A$
	J	$0.5\,Ah^2$	$2/3\,Ah^2$	$1\,Ah^2$
	W	$A\,h$	$A\,h$	$3\,A\,h$
With deck	y_G	$\frac{A_d+A}{2 \cdot A+A_d} \cdot h$	$\frac{A_d+2 \cdot A}{3 \cdot A+A_d} \cdot h$	$\frac{A_d+A}{3 \cdot A+A_d} \cdot h$
	J	$J_D + A_d \cdot \left(\frac{h}{2}\right)^2 + +A \cdot (h - y_G)^2 + A \cdot {y_G}^2$	$J_D + A_d \cdot \left(\frac{h}{2}\right)^2 + +2 \cdot A \cdot (h - y_G)^2 + A \cdot {y_G}^2$	$J_D + A_d \cdot \left(\frac{h}{2}\right)^2 + +A \cdot (h - y_G)^2 + 2 \cdot A \cdot {y_G}^2$

A_t =whole gross area of chords; h= distance between chords.

For the deformability assessment, according to creep coefficient values provided by CNR-DT 205 [11], the elastic modulus E_1 was reduced through a factor of 0.66, and shear modulus G through a factor 0.448 (considering shear deformation), to account for long-term effects, assuming an average service life of 10 years, while the material strength was reduced by the safety coefficient g = 1.35 × 1.15. Creep effects are evaluated in accordance with the relevant literature [11,14] using the *Effective Modulus Method*, by introducing the adopted creep coefficients to modify the elastic moduli according to the following expressions: $E_{\text{eff}} = E_1/(1 + \varphi_E)$ and $G_{\text{eff}} = G/(1 + \varphi_G)$, where different creep coefficients are considered for longitudinal behavior (φ_E) and shear behavior (φ_G). Comparable reduction factors are also suggested in ASCE/SEI 74 [14]. Parameter c $=1/k$ is the shear factor for the cross-section, which is about 2 for the present case of circular hollow profiles.

In the definition of the transverse width of the deck (base b), it has been assumed that the minimum value is between $L/12$ and $i/2$ (where i is the spacing of longitudinal beams). This assumption can be justified through numerical and parametric analyses like the one carried out in the next section.

By considering the geometric characteristics of a beam with a deck as a function of one without a deck by an increasing factor of 3.33 for the inertia of 3.33 (that is, a mean value for the truss with a span between 10 and 25), it is possible to easily derive the ratio L/h with respect to a prefixed deflection $\delta_0 = L/\beta$ with the following expression:

$$3.33 \cdot \frac{A \cdot h^2}{4} = \frac{L^3}{48 \cdot E} \cdot \frac{\beta}{L} \cdot \left(\frac{5}{8} \cdot q_{SLS} \cdot L + P_{SLS}\right) \tag{14}$$

Equation (14) was derived from Equation (13) combined with the expression of inertia assumed as the value J = 3.33 $A\,h^2/2$.

By solving Equation (14) with respect to *L/h*, a simple expression of *L/h* is found as a function of span length *L* for established values of geometric properties and loads:

$$\frac{L}{h} = 6.32 \cdot \sqrt{\frac{E \cdot A}{\beta} \cdot \frac{1}{(5/8 \cdot q_{SLS} \cdot L + P_{SLS})}} \tag{15}$$

From a dynamic perspective, considering a simply supported beam with a distributed mass density q, the first frequency is given by

$$f_1 = \frac{\pi}{2}\sqrt{\frac{E_1\,J}{q\,L^4}} \tag{16}$$

According to the indications on the design of FRP bridges (and for lightweight structures and slender footbridges), the fundamental frequency must be greater than 5 Hz (period less than 0.2 s) for vertical vibrations and 2.5 Hz (period 0.1 s) for flexural and torsional vibrations. If the fundamental frequency is less than 3 Hz (period 0.33 s) for horizontal or torsional vibrations, the use of dampers is recommended. From these limits, it is possible to find an optimal value of D/t for main elements which meet the static and dynamic requirements. Specifically, adopting a circular cross-section of diameter D = 180 mm and thickness 10 mm results in D/t = 18, for which the strength in compression comes from the material and is not reduced by buckling effects (see Table 2 for limit of D/t).

In this paper, solution (a) in Table 3 is mainly investigated, because it is a plane truss scheme, simply assembled on site with adjacent beams and an upper deck panel, in order to form the bridge deck. Figure 9 shows, for the truss configuration in case (a) in Table 3, the variation in required *h* for strength requirement (Figure 9a, design compressive strength σ_m = 300/1.49) and maximum deflection requirement (Figure 9b, 1/300 *L*) for the characteristic combination of permanent + moving loads, by varying the span length *L* of the bridge (E_1 = 30 GPa, E_2 = 1/3 E_1, G = 1/9 E_1) and considering design load increasing factor g_q = 1.35 according to Eurocode 1 for ULS loads.

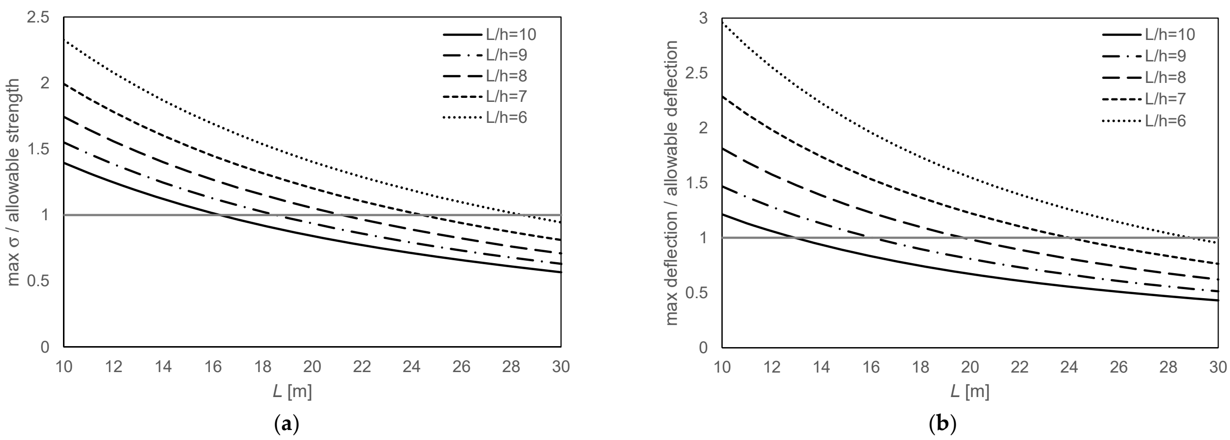

Figure 9. Diagrams of ratios in terms of strength and deflection varying with span length. (**a**) Ratio between maximum stress and material strength; (**b**) ratio between maximum deflection and allowable deflection.

It is worth noting that deflection is penalized by the point loads, whose characteristic value is very high, considering the service life of these bridges; hence, a more realistic deflection value for the sizing of pultruded elements could be the one related to the frequent live load combination, limiting them to the value of 1/400 L or 1/500 L.

The analysis of the design graphs in Figure 9 indicates that, for GFRP bridges, serviceability, and specifically deflection, is the governing criterion for spans up to 25 m.

The results shown in Figure 9 are summarized in Figure 10 through two curves, for strength check and deflection check, in which variation in L/h is considered by span length. To satisfy the deflection limits, the required beam height results in an L/h ratio between 15 and 7 for spans ranging from 10 to 25 m when considering strength verification. When deflection is checked under the limit of 1/300 L and long-term effects such as viscoelastic deformation are considered, the corresponding L/h ratios decrease further, falling between 11 and 6.5. By increasing the deformability limit to 1/500 L for the characteristic combination, the range of acceptable L/h ratios reduces, falling between 9 and 5. This demonstrates that, for medium-span GFRP bridges, long-term deflection controls the design, rather than material strength.

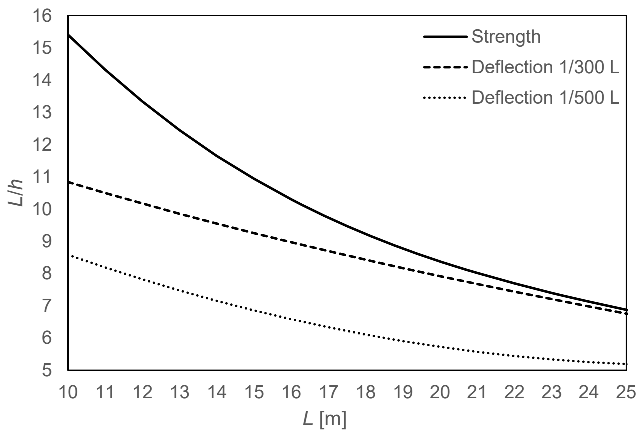

Figure 10. Required ratio L/h versus L in terms of strength and deflection.

A comparative assessment was then performed for bridges built with different materials: steel–concrete composite, prestressed concrete, and pultruded GFRP, considering the same dead and permanent loads, including 2 kN/m^2 for the roadway superstructure. The design of each bridge type was carried out following the safety factors recommended by the relevant codes: CNR-DT 205 [11] for GFRP, Eurocode 3 for steel structures, and Eurocode 2 for prestressed concrete.

For the prestressed concrete bridge, the slab thickness was set to 30 cm, supported by six prestressed concrete beams with a base width of 60 cm and a depth corresponding to $h = L/15$, or a bridge width of 9 m. For the steel-composite bridge, four longitudinal girders were used, each constituting W-shaped beams with top and bottom flanges 60 cm wide and 2.5 cm thick, and webs 1.8 cm thick, with a depth ratio of $h = L/9$.

For the GFRP bridge, six longitudinal beams were adopted, with the L/h ratio determined according to the proposed design model, in order to satisfy both strength and serviceability requirements, and the top deck thickness was set to 300 mm. The comparison highlights that, while traditional materials like steel and prestressed concrete are primarily governed by strength for these spans, the design of GFRP bridges is strongly controlled by deflection, particularly when long-term effects are included. This emphasizes the importance of accurate long-term deflection prediction in the preliminary and final design of pultruded GFRP bridges.

The comparison (Figure 11) highlights the relative lightness of GFRP bridge solutions compared to their concrete or steel counterparts. However, this advantage must be carefully assessed in terms of bridge vibrations under dead load, member slenderness and overall deflection under loads.

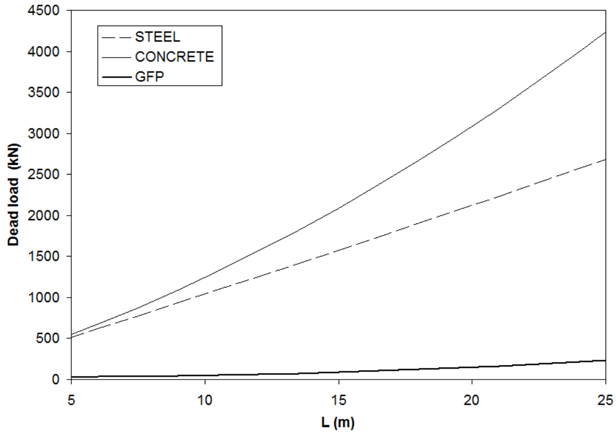

Figure 11. Dead load of prestressed concrete, steel and GFRP bridges versus span *L*.

According to CNR-DT 205, in long-term design conditions, the reduction factors associated with fatigue verification are not applied simultaneously, as they are not additive. In the present study, long-term effects have therefore been taken into account, while fatigue phenomena in the structural members have not been explicitly considered. This assumption is justified by the fact that repetitive loads induce limited variations in the stress state. Consequently, the cyclic stress ranges remain well below the expected residual fatigue strength of the materials, which is generally assumed to be equal to half of the nominal strength (f_{fat}= 0.5 f_{y}), from the consistent Wöhler curve [40].

3.2. Numerical Analysis

In this section, the results obtained on FE models of the proposed bridge are reported, through a parametric study, by varying the span length and the corresponding L/h ratio. Views of the reference model are shown in Figure 12.

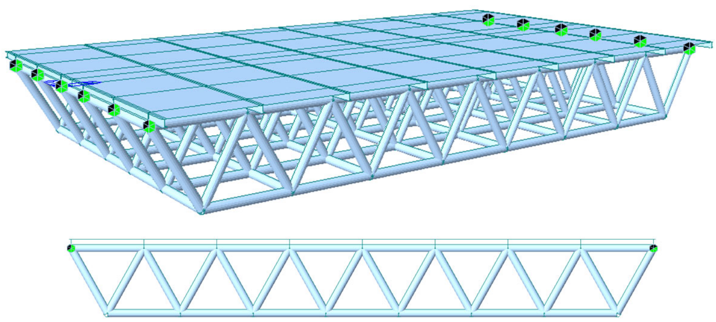

Figure 12. The 3D FE model. General view and lateral view of the reference model.

The reference case is a bridge with a span length of 16 m, characterized by a deck width of 9.5 m. The truss members have circular cross-sections with a diameter of 210 mm and a wall thickness of 15 mm, while the overall truss depth is equal to 1.8 m (L/h = 8.9). The deck consists of pultruded GFRP elements spanning 1.5 m between the load-bearing trusses. The deck configuration includes top and bottom flanges with a thickness of 6 mm and webs of 6 mm, arranged at a pitch of 75 mm, 200 mm thick. The material properties adopted in the analysis correspond to an elastic modulus E_1 = 30 GPa, with E_2 = $E_1/3$ and shear modulus G = $E_1/9$. For road bridges, the design moving loads of Eurocode 1 [39] for the heaviest traffic lane are considered (uniform load 9 kN/m^2 for the 3 m lane width and tandem point load of 300 kN each). Superimposed dead loads due to pavement and facilities are assumed to be distributed with the value of 2 kN/m^2.

The numerical models of four different bridges, based on the reference analytical model, are performed through MIDAS CIVIL software v. 2024 for three cases, by varying span and span/height ratio. The properties of FE models are reported in Table 4.

Table 4. Properties of FE bridge models.

Span Length (L) [m]	Truss Height (h) [m]	L/h	Nodes	Beam Elements	Shell Elements
12	1.20	10	141	325	48
16	1.80	8.9	183	421	64
20	2.50	8.0	225	517	80
24	3.60	6.7	267	589	96

Beam elements are used for truss members while shell elements are used to model the deck. Orthotropic material, with different properties for long-term and short-term load conditions, was defined. Simply supported boundary conditions are applied at the truss ends. The deck is assumed to be rigidly connected to the lower truss structure, ensuring full composite action between the deck and the supporting truss.

In the model, the joints are assumed to be rigid, as the selected connection detail exhibits high flexural stiffness as well as axial stiffness significantly greater than that of the connected members. The assumption of linear joint behavior is justified by the very low axial force levels resulting from the limitation imposed by member buckling criteria, which leads to low stress levels within the connections. Under these conditions, modeling the joints as rigid is considered appropriate for the case under study.

Furthermore, in the presence of an orthotropic deck—characterized by different elastic moduli in the principal directions, as well as varying sectional areas and moments of inertia depending on its constituent elements—a rigid connection can reasonably be assumed through the use of load-distribution plates designed to prevent local punching phenomena.

Alternative connection modeling strategies should be introduced only through refined local models of the joint and supported by dedicated experimental testing. Such investigations are beyond the scope of the present study but represent a relevant direction for future research.

Results in terms of deformed configuration and axial stress in the truss members are shown in Figure 13 for the reference model of 16 m and in Table 5 for the three cases analyzed.

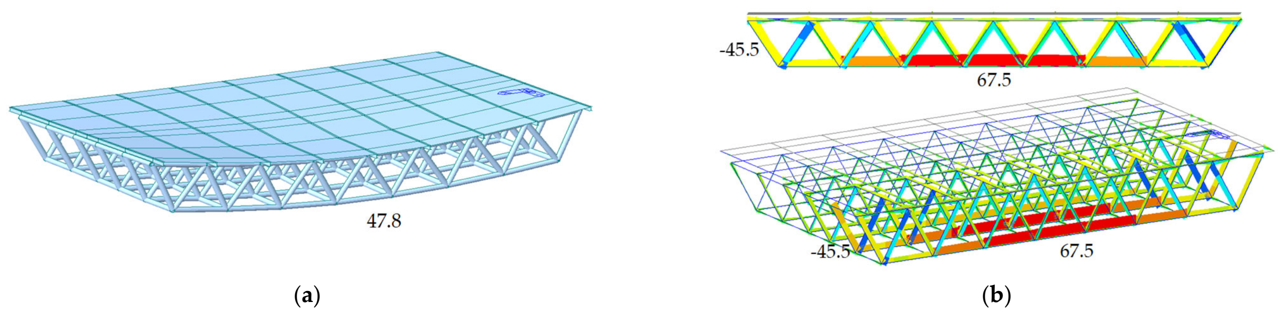

Figure 13. Results obtained on FE model (reference with span L = 16 m). (**a**) Deflection (mm); (**b**) axial stress distribution in truss members in ULS (MPa).

Table 5. Results of FE models.

Span Length (L) [m]	Deflect. δ FE Char. [mm]	Deflect. δ FE Freq. [mm]	δ/L FE Char.	Max Deflect. Analytical δ [mm]	Def. Error FE/Anal. [%]	Max Compr. Stress σ_{ULS} [MPa]	σ_{ULS}/σ_{cr}	λ	1st Freq. [Hz]
12	32.3	23.4	1/371	37.7	−14.3%	40.1	0.055	17	13.58
16	47.8	34.8	1/335	52.1	−8.2%	45.5	0.062	25	10.35
20	64.8	47.5	1/309	67.0	−3.3%	50.2	0.065	35	8.38
24	79.7	58.7	1/302	74.8	6.5%	56.6	0.078	49	7.19

Results achieved through the FE models confirm the adopted sizing and design choices, as all the prescribed limits are satisfied. In particular, the checks are fulfilled both in terms of maximum compressive stress, with respect to local buckling and global instability, and in terms of serviceability requirements, namely, the deflection limits. The average discrepancy between deflections predicted by the analytical model and those obtained from the numerical simulation is approximately 5%. Nevertheless, it is strongly dependent on span, with smaller spans typically showing lower overall deformability.

The results also highlight an improvement in the stress and deformation response compared to those predicted by the two-dimensional analytical model and by the previously adopted simplified approaches. This enhancement is attributed to the three-dimensional structural behavior, which allows for transverse redistribution of the actions on the deck and internal forces among the structural members, as well as to the inertial contribution of the composite deck–truss with respect to the truss girder. Such interaction promotes a more effective collaboration between the truss elements and the upper deck surface, leading to a more favorable global structural response.

Figure 14 shows a comparison between results from FE models and the analytical procedure seen above; the diagrams indicate the values of deflection respect to the limit set to $L/333$ in terms of L/h ratios of the four parametric models and the value of maximum compressive stress with respect to the one computed in the analytical model for the same truss. It can be observed that the results obtained from the finite element model are in good agreement with the analytical ones, in terms of the selection of the L/h ratio that ensures the limit deflection and the corresponding maximum compressive stress in the strut.

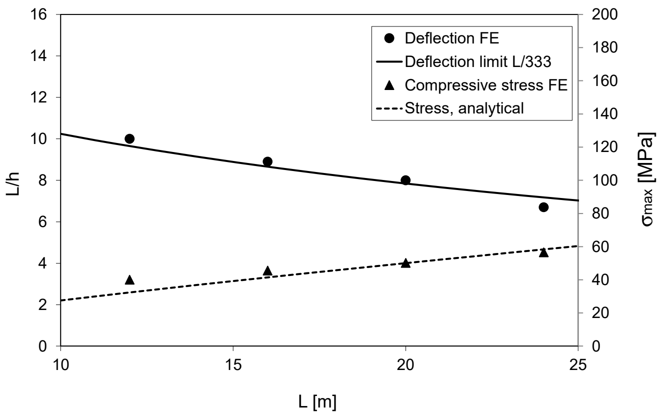

Figure 14. Comparison of results achieved with FE models and analytical procedure for deflection and maximum compressive stress in the truss struts.

Figure 15 shows results in terms of expected deflection for the characteristic load and frequent load combinations, compared to the limit values of $L/300$ and $L/500$. In particular, Figure 15a shows that the L/h ratios selected for the beam models are adequate to satisfy the maximum deflection requirement for the characteristic load combination. Conversely, Figure 15b shows the deflection values obtained for the two load combinations with respect to the allowable deflection range between $L/300$ and $L/500$ of the span. It can be observed that all the results fall within the deformability range required in the SLS. Moreover, the FE model is generally stiffer than the analytical one, as it accounts for adjacent beams and the possible transverse load redistribution promoted by the rigid connection between the deck and the circular pultruded profiles in the three-dimensional deck configuration.

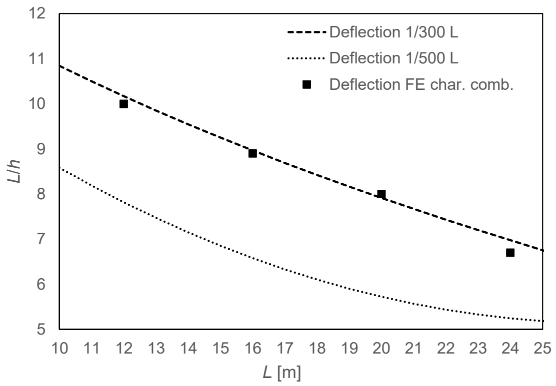

(**a**)

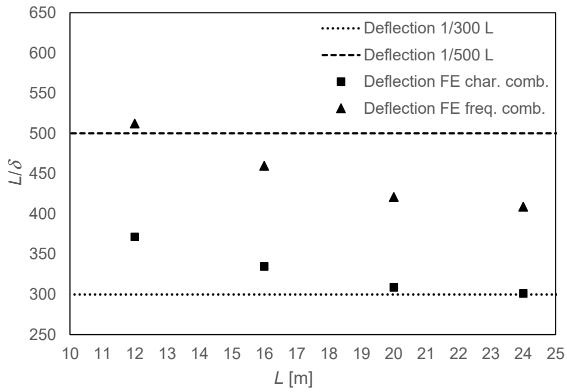

(**b**)

Figure 15. Comparison of results achieved with FE models in terms of deflection with limits established in the analytical approach. (**a**) Deflection of FE models with respect to L/h ratio; (**b**) deflection for characteristic and frequent combination of live loads with respect to L/d ratio.

Figures 14 and 15 can be readily used within the framework of preliminary design to determine from the outset the appropriate height of the trussed girder relative to the bridge span in order to satisfy deflection limits, given that the height required to meet these limits varies nonlinearly with the span.

Figure 16 shows a comparison between the frequencies obtained using the analytical method through Equation (16) and those derived from the FE model; in this case, as well, a good agreement with the expected frequencies is observed, considering that the analytical evaluation performed on a simply supported beam with an equivalent inertia section is approximate compared to the results obtained from the 3D model with the actual mass distribution.

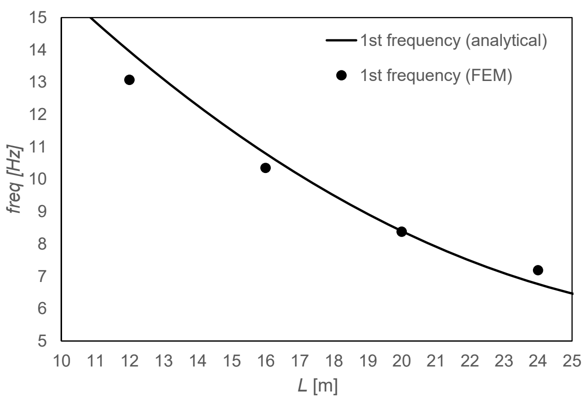

Figure 16. Comparison of 1st frequency achieved with FE models and analytical approach.

In this study, a comparison was performed between the sizing of bridge decks with main beams modeled in a planar configuration and 3D models with adjacent beams as a first-level design approach. More advanced spatial beam approaches, which enable enhanced transverse interaction, could also be adopted through the design procedures based on the simplified schemes (b) and (c) illustrated in Table 3. The implementation of these approaches constitutes a promising direction for further studies.

3.3. Sequence of Design Stages Through the Proposed Procedure

The proposed procedure can be summarized into two distinct phases: an initial preliminary sizing phase, followed by a second phase involving numerical analysis and verification in terms of strength, deformability, and related performance criteria. Figure 17 presents the corresponding summary flowchart, schematically illustrating the entire procedure.

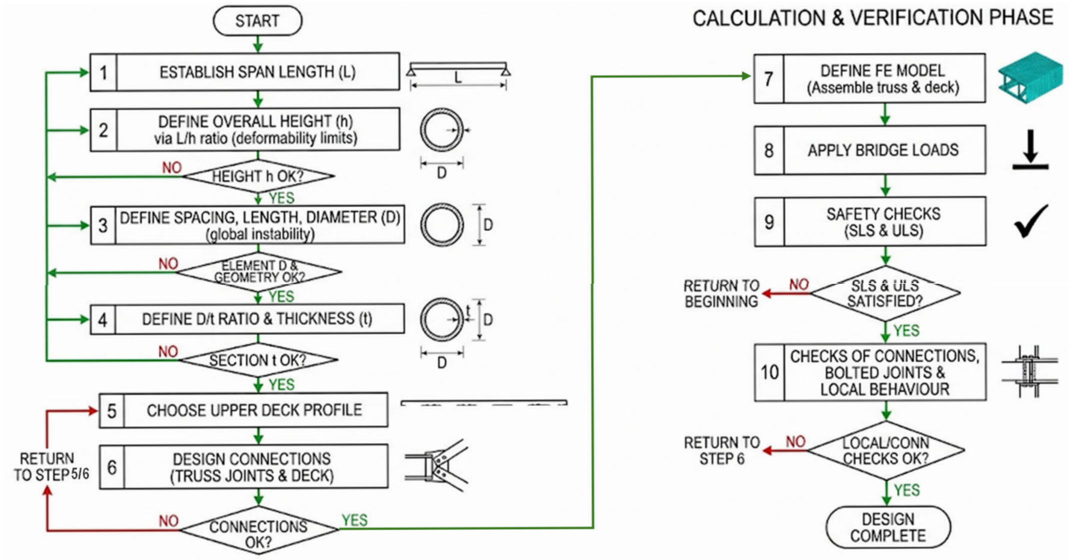

Figure 17. Trussed bridge design and verification flowchart.

The first phase enables the preliminary dimensioning of structural elements to satisfy the prescribed limits in terms of local and global stability, overall deformability, and the strength of both members and connections. The second phase provides a more detailed verification under dead and live loads, as well as the definition of construction stages and refined analyses of connection behavior.

The preliminary design phase is therefore subdivided into several additional stages, each addressing a specific phenomenon that defines a governing dimensional limit. This approach makes it possible to identify an optimal solution to be subsequently implemented in the numerical model for the final analysis. In this framework, optimization is primarily carried out during the preliminary design stage, balancing different performance requirements at both the local and global levels, under the assumption of a predefined truss configuration with repetitive members that allow straightforward assembly using identical elements and standardized joints.

An alternative approach would involve optimizing the material on a member-by-member basis; however, this would significantly complicate fabrication and erection, requiring elements with varying geometric properties and different connection details, which is not the strategy adopted in this study.

Nevertheless, the proposed procedure can be automated by implementing the previously defined design relationships within each sub-stage, enabling automatic or semi-automatic sizing as key parameters—such as span length or deck width—to vary. This approach was implemented through the flowchart presented in Figure 17 for the parametric cases examined and implemented in the different finite element models developed in the previous section.

4. Conclusions

This study investigated the replacement of aging short- and medium-span reinforced concrete bridges using lightweight GFRP truss deck systems while preserving existing piers and foundations. The proposed solution, based on pultruded GFRP beams and decks, substantially reduces structural mass, decreasing seismic demand and lateral forces on substructures, and is suitable for both permanent and temporary bridge applications, including rapid deployment scenarios.

A two-stage design and assessment procedure was adopted. In the first stage, preliminary analytical sizing methods guided the selection of structural typology, the definition of truss member cross-sectional properties, and the development of efficient connection strategies ensuring rapid assembly and adequate joint overstrength. Strength, deformability, local buckling, and global instability due to member slenderness were explicitly considered. In the second stage, detailed three-dimensional finite element simulations were conducted to evaluate global deformability, load redistribution, stress patterns, and the interaction between primary beams and deck panels. A parametric study varying span length and girder *L/h* ratio allowed for direct validation of the analytical sizing approach against refined numerical models, confirming its reliability for preliminary design.

The main findings provide practical guidance for defining the fundamental design parameters of GFRP truss deck structures capable of satisfying both strength and serviceability limits:

- Height-to-span ratio (h/L): For spans between 10 and 25 m, a minimum h/L ratio between 1/10 and 1/6 ensures compliance with the L/300 deflection limit under characteristic loads, while maintaining a vertical vibration period below 0.3 s. Long-term creep effects and shear deformation contributions are included, and vibration mitigation devices may be necessary in specific cases.
- Truss geometry and chord slenderness: Spatial truss configurations with two upper circular chords are effective, though potentially costly. The diameter-to-thickness ratio should not exceed 40, and maximum geometric slenderness should be limited to 45 to prevent local buckling and ensure adequate structural performance.
- Deflection and serviceability: Bridges with limited service life (e.g., 10 years) more easily satisfy serviceability limits due to reduced long-term effects and shorter sustained loading duration.
- Joint design: Bolted steel plates combined with bonded steel–GFRP interfaces provide sufficient overstrength and support modular, factory-controlled assembly.

Overall, the integrated analytical–numerical framework validated in this study constitutes a practical tool for preliminary design, enabling designers to determine the key structural parameters of truss deck systems that meet both strength and deformability requirements. The principal novelty of this work lies in extending design concepts traditionally applied to pedestrian bridges to short- and medium-span road bridges, demonstrating that GFRP truss decks can provide lightweight, efficient, and reliable alternatives to conventional concrete or steel solutions, suitable for permanent rehabilitation as well as temporary or emergency applications.

Author Contributions: Conceptualization, methodology, validation, formal analysis, investigation, data curation, writing—original draft preparation, writing—review and editing, G.C. Methodology, validation, investigation, data curation, writing—review and editing, M.F.G. All authors have read and agreed to the published version of the manuscript.

Funding: This paper received no funding.

Data Availability Statement: Data are available from the author on reasonable request.

Conflicts of Interest: The authors declare no conflicts of interest.

References

1. Bank, L.C. *Composites for Construction: Structural Design with FRP Materials*; Wiley: Hoboken, NJ, USA, 2006. [CrossRef]
2. Keller, T. Overview of Fibre-Reinforced Polymers in Bridge Construction. *Struct. Eng. Int.* **2002**, *12*, 66–70. [CrossRef]
3. Bank, L.C.; Mahoney, C.R.; Keller, T. Design of GFRP pedestrian bridges: Case studies and practical guidance. *J. Bridge Eng.* **2014**, *19*, 06014001.
4. Campione, G. Strength and stability of pultruded GFRP elements. *Results Eng.* **2025**, *26*, 105158. [CrossRef]
5. Hollaway, L. *Advanced Fibre-reinforced Polymer (FRP) Composites for Structural Applications*; Elsevier: Oxford, UK, 2022; ISBN 9780128203460.
6. Živanović, S.; Pavić, A.; Reynolds, P. Vibration serviceability of footbridges under human-induced excitation: A literature review. *J. Sound Vib.* **2005**, *279*, 1–74. [CrossRef]
7. Bai, Y.; Yang, X. Novel Joint for Assembly of All-Composite Space Truss Structures: Conceptual Design and Preliminary Study. *J. Compos. Constr.* **2013**, *17*, 130–138. [CrossRef]
8. Campione, G. Comparison Between Pedestrian and Road Bridges Designed with GFRP Pultruded Trusses. *Bridge Eng. Rep.* **2026**, *3*, 70. [CrossRef]
9. Eurocomp. *European Guidelines for the Design of FRP Structures*; ECCS: Brussels, Belgium, 1996.
10. *Guidelines for FRP Structural Applications in Bridges*; Highway Structures and Bridge Design; Department for Transport: London, UK, 2005.
11. Consiglio Nazionale delle Ricerche (CNR) 2008. CNR-DT 205/2007 Istruzioni per la Progettazione, l'Esecuzione ed il Controllo di Strutture realizzate con Profili Pultrusi di Materiale Composito Fibrorinforzato (FRP). (In Italian). Available online: https://www.cnr.it/it/node/2625 (accessed on 29 March 2026).
12. AASHTO. *LRFD Load and Resistance Factor Design Specifications for FRP Bridges*; American Association of State Highway and Transportation Officials: Washington, DC, USA, 2010.
13. AASHTO. *Standard Specifications for Structural Supports for Highway Signs, Luminaires, and Traffic Signals*, 6th ed.; American Association of State Highway and Transportation Officials: Washington, DC, USA, 2013.
14. *ASCE/SEI 74*; Guidelines for the Design of FRP Structural Members. American Society of Civil Engineers: Reston, VA, USA, 2023.
15. *CEN/TS 19101:2022*; Design of Fibre-Polymer Composite Structures. CEN (European Committee for Standardization): Brussels, Belgium, 2022.
16. *T/CECS 692-2020*; Technical Specification for Structure of Pultruded Fiber Reinforced Polymer Composites. China Engineering Construction Standardization Association: Beijing, China, 2020.
17. Yang, X.; Bai, Y.; Ding, F. Structural performance of a large-scale space frame assembled using pultruded GFRP composites. *Compos. Struct.* **2015**, *133*, 986–996. [CrossRef]
18. Zhu, R.; Li, F.; Shao, F.; Zhang, D. Static and dynamic behaviour of a hybrid PFRP-aluminium space truss girder: Experimental and numerical study. *Compos. Struct.* **2020**, *243*, 112226. [CrossRef]
19. Barbero, E.; Tomblin, J. A phenomenological design equation for FRP columns with interaction between local and global buckling. *Thin-Walled Struct.* **1994**, *18*, 117–131. [CrossRef]
20. Puente, I.; Insausti, A.; Azkune, M. Buckling of GFRP Columns: An Empirical Approach to Design. *J. Compos. Constr.* **2006**, *10*, 529–537. [CrossRef]
21. Pecce, M.; Cosenza, E. Local buckling curves for the design of FRP profiles. *Thin-Walled Struct.* **2000**, *37*, 207–222. [CrossRef]
22. Higgoda, T.M.; Elchalakani, M.; Kimiaei, M.; Wittek, A.; Yang, B. Flexural behaviour of pultruded circular tubular GFRP composite truss bridges with novel non-corrosive connections. *Structures* **2022**, *45*, 830–853. [CrossRef]
23. Chen, W.; Li, Y.; Yang, J. Experimental investigation on bolted and bonded GFRP truss connections. *Compos. Struct.* **2022**, *289*, 115511. [CrossRef]
24. Nettis, A.; Nettis, A.; Ruggieri, S.; Uva, G. Corrosion-induced fragility of existing prestressed concrete girder bridges under traffic loads. *Eng. Struct.* **2024**, *314*, 118302. [CrossRef]
25. Granata, M.F.; Recupero, A.; Culotta, G.; Arici, M. Influence of axial force and corrosion on failure of prestressed concrete structures considering M-V interaction. *Eng. Struct.* **2021**, *242*, 112552. [CrossRef]
26. Kim, H.-Y.; Park, K.-T.; Jeong, J.; Lee, Y.-H.; Hwang, Y.-K.; Kim, D. A pultruded GFRP deck panel for temporary structures. *Compos. Struct.* **2009**, *91*, 20–30. [CrossRef]
27. Zhang, H.; Li, F. A review of prediction methods for global buckling critical loads of pultruded FRP struts. *Compos. Struct.* **2024**, *329*, 117752. [CrossRef]
28. Zhang, C.; Chen, Y.; Dou, M. Axial Compression Behaviour and Modelling of Pultruded Basalt-Fibre-Reinforced Polymer (BFRP) Tubes. *Buildings* **2023**, *13*, 1397. [CrossRef]
29. Teixeira, A.M.A.J.; Pfeil, M.S.; Battista, R.C. Structural evaluation of a GFRP truss girder for a deployable bridge. *Compos. Struct.* **2014**, *110*, 29–38. [CrossRef]

30. Hizam, R.M.; Manalo, A.C.; Karunasena, W.; Bai, Y. Effect of bolt threads on the double lap joint strength of pultruded fibre reinforced polymer composite materials. *Constr. Build. Mater.* **2018**, *181*, 185–198. [CrossRef]
31. Hizam, R.M.; Manalo, A.C.; Karunasena, W.; Bai, Y. Behaviour of pultruded GFRP truss system connected using through-bolt with mechanical insert. *Compos. Part B Eng.* **2019**, *168*, 44–57. [CrossRef]
32. Bačinskas, D.; Rimkus, A.; Rumšys, D.; Meškėnas, A.; Bielinis, S.; Sokolov, A.; Merkevičius, T. Structural Analysis of GFRP Truss Bridge Model. *Procedia Eng.* **2017**, *172*, 68–74. [CrossRef]
33. Cardoso, D.C.T.; Harries, K.A.; Batista, E.D.M. Compressive strength equation for GFRP square tube columns. *Compos. Part B Eng.* **2014**, *59*, 1–11. [CrossRef]
34. Timoshenko, S.P.; Gere, J.M. *Theory of Elastic Stability*; McGraw-Hill: New York, NY, USA, 1961.
35. Yazhini, A.; Ramesh, B.C. Behavior of circular glass fiber reinforced polymer tubes under axial compression. *Int. J. Sci. Eng. Appl.* **2015**, *4*, 110–116. [CrossRef]
36. Yousif, K.; Dean, A.; Mahdi, E. Crushing behavior of GFRP composite-reinforced PVC tubes: Experimental testing and numerical simulation. *Compos. Sci. Technol.* **2024**, *258*, 110903. [CrossRef]
37. Hao, X.; Zhu, R.; Li, R.; Li, F. Effect of Joint Stiffness on Flexural Performance of a Hybrid FRP-Aluminum Space Truss Structure. *J. Struct. Eng. ASCE* **2021**, *147*, 04021214. [CrossRef]
38. Qiu, C.; Bai, Y.; Zhang, L.; Jin, L. Bending Performance of Splice Connections for Assembly of Tubular Section FRP Members: Experimental and Numerical Study. *J. Compos. Constr.* **2019**, *23*, 04019040. [CrossRef]
39. *EN 1991-2*; Traffic Loads on Bridges, Part 2. CEN (European Committee for Standardization): Brussels, Belgium, 2005.
40. Bezazi, A.; El Mahi, A.; Berthelot, J.-M.; Kondratas, A. Investigation of Cross-Ply Laminates Behaviour in Three Point Bending Tests. Part II: Cyclic Fatigue Tests. *Mater. Sci. (Medžiagotyra)* **2003**, *9*, 128–133.